Biologicals 80 (2022) 18–26

Contents lists available at ScienceDirect

Biologicals

journal homepage: www.elsevier.com/locate/biologicals

Adjuvant effect of mesoporous silica SBA-15 on anti-diphtheria and anti-tetanus humoral immune response

Aryene Góes Trezena [a], Pedro Leonidas Oseliero Filho [b], Luís Carlos Cides da Silva [b], Cristiano Luis Pinto Oliveira [b], José Luiz de Souza Lopes [b], Nayara da Silva Antonio [a], Viktor Fonseca Barbosa Dettmann [a], Milena Apetito Akamatsu [c], Tereza da Silva Martins [d], Orlando Garcia Ribeiro [a], Márcia Carvalho de Abreu Fantini [b], Osvaldo Augusto Sant'Anna [e], Milene Tino-De-Franco [a,*]

[a] Immunogenetics Laboratory, Butantan Institute, São Paulo, SP, Brazil
[b] Physics Institute, University of São Paulo, SP, Brazil
[c] Bioindustrial Center, Butantan Institute, São Paulo, SP, Brazil
[d] Chemistry Department, Federal University of São Paulo, Diadema, SP, Brazil
[e] Immunochemistry Laboratory, Butantan Institute, São Paulo, SP, Brazil

ARTICLE INFO

Keywords:
Adjuvant
Ordered mesoporous silica SBA-15
Diphtheria anatoxin
Tetanus anatoxin
Combined vaccines

ABSTRACT

Routine immunization against diphtheria and tetanus has drastically reduced the incidence of these diseases worldwide. Anti-diphtheria/tetanus vaccine has in general aluminum salt as adjuvant in its formulation that can produce several adverse effects. There is a growing interest in developing new adjuvants. In this study, we evaluated the efficiency of SBA-15 as an adjuvant in subcutaneous immunization in mice with diphtheria (dANA) and tetanus (tANA) anatoxins as well as with the mixture of them (dtANA). The tANA molecules and their encapsulation in SBA-15 were characterized using Small-Angle X-ray Scattering (SAXS), Dynamical Light Scattering (DLS), Nitrogen Adsorption Isotherm (NAI), Conventional Circular Dichroism (CD)/Synchrotron Radiation Circular Dichroism (SRCD) Spectroscopy, and Tryptophan Fluorescence Spectroscopy (FS). The primary and secondary antibody response elicited by subcutaneous immunization of High (H_{III}) and Low (L_{III}) antibody responder mice with dANA, tANA, or dtANA encapsulated in the SBA-15 were determined. We demonstrated that SBA-15 increases the immunogenicity of dANA and tANA antigens, especially when administered in combination. We also verified that SBA-15 modulates the antibody response of L_{III} mice, turning them into high antibody responder. Thus, these results suggest that SBA-15 may be an effective adjuvant for different vaccine formulations.

1. Introduction

Diphtheria and tetanus are potentially lethal diseases caused by toxins produced by *Corynebacterium diphtheriae* and *Clostridium tetani,* respectively. While diphtheria is a respiratory infection characterized by a membranous inflammation of the pharynx, larynx, and trachea [1], tetanus is a neurological disorder where presynaptic membranes at neuromuscular junctions are affected by the bacteria toxin, which results in the characteristic spasms [2].

Since 1948, vaccines containing both diphtheria and tetanus anatoxins have been used to immunize adults and children worldwide. In addition, it has already been demonstrated that combinations of different components enhance the immune response to specific antigens in the presence of aluminum salts as an adjuvant [3]. Despite the common use of aluminum salts (as aluminum hydroxide and aluminum phosphate), along other compounds like calcium phosphate in licensed vaccines [4,5], aluminum adjuvants are responsible for some undesirable side effects like swelling, induration, erythema, induction of allergy

* Corresponding author. Immunogenetics Laboratory, Butantan Institute. Av. Vital Brasil, 1500, São Paulo, SP, 05503-900, Brazil.
E-mail addresses: aryene.trezena@butantan.gov.br (A.G. Trezena), pedroleonidasoseliero@hotmail.com (P.L. Oseliero Filho), luiscides@gmail.com (L.C. Cides da Silva), crislpo@if.usp.br (C.L.P. Oliveira), zeluiz@if.usp.br (J.L.S. Lopes), naya.antoni@gmail.com (N.S. Antonio), viktor.dettmann@butantan.gov.br (V.F.B. Dettmann), milena.akamatsu@butantan.gov.br (M.A. Akamatsu), tsmartins@unifesp.br (T.S. Martins), orlando.ribeiro@butantan.gov.br (O.G. Ribeiro), mfantini@if.usp.br (M.C.A. Fantini), osvaldo.santanna@butantan.gov.br (O.A. Sant'Anna), milene.tino@butantan.gov.br (M. Tino-De-Franco).

https://doi.org/10.1016/j.biologicals.2022.10.001
Received 22 March 2022; Received in revised form 25 July 2022; Accepted 25 October 2022
Available online 19 November 2022

and autoimmune reaction [6–8]. Besides, aluminum salts induce mainly TH2 [9] responses, being less efficient in vaccines against diseases that involve predominantly a TH1-like response Thus, it would be suitable and relevant to develop novel adjuvant candidates less harmful, economically viable, chemically stable, and effective in immunocompromised people.

The ordered mesoporous silica (OMS) SBA-15 [10] has been studied as an adjuvant due to its specific physical and structural properties. Its pores enable efficient loading of antigen with a high loading capacity [11,12]. In recent years, a number of studies conducted by our group demonstrated the SBA-15 adjuvant properties in animal models. Several antigens were used as *E. coli* bacterial protein (Int1β) and Micrurus snake venom [13], bovine serum albumin (BSA) [14] and HBsAg from the Hepatitis B virus [15].

Two heterogeneous lines of mice were produced by bidirectional selective breeding based on the quantitative antibodies production to the flagellar antigen of *Salmonella enterica* serotype Typhimurium and called Selection III [16–18]. Two High (H_{III}) and low (L_{III}) antibody responder line of mice constitute an adequate model for the study of immune responsiveness [19], infectious diseases [20–22] and vaccine efficacy [23]. The experimental use of these genetically heterogeneous mice brings the investigation closer to what is observed in the human population. For this reason, H_{III} and L_{III} mouse lines were used as a suitable model for the assessment of the efficacy of vaccine processes.

The present study evaluates the effectiveness of SBA-15 as adjuvant in the humoral response to subcutaneous immunization with diphtheria anatoxin (dANA), tetanus anatoxin (tANA) and combined anatoxins (dtANA) in both H_{III} and L_{III} mouse lines. The characterization data for dANA have already been published by our group [24] so in this study we focused our efforts in the characterization of tANA macromolecules and their encapsulation into SBA-15. Small-Angle X-ray Scattering (SAXS), Dynamical Light Scattering (DLS), Nitrogen Adsorption Isotherm (NAI), Conventional Circular Dichroism (CD)/Synchrotron Radiation Circular Dichroism (SRCD) spectroscopy and Tryptophan Fluorescence Spectroscopy (FS) were used.

SAXS and DLS measurements of pure antigens dispersed in buffer solution provided information on their typical dimensions and aggregation state, which is limiting for their encapsulation inside the SBA-15 mesopores. Moreover, variations in the SAXS curves obtained for the immunogenic complexes SBA-15+anatoxins are indicative of protein encapsulation. These results agreed with NAI results, which by comparing the pristine silica with the samples containing the antigens showed variations of surface area, pore's volume and pore's diameters. CD/SRCD and FS results confirmed the protein integrity after encapsulation. Our biological results indicate that a higher antibody response could be achieved in both H_{III} and L_{III} mouse lines with a combined immunization with both antigens encapsulated in SBA-15. We also demonstrated that OMS SBA-15 increases the immunogenicity and modulates the antibody response of L_{III}, turning them into a high antibody responder to dANA and tANA antigens.

2. Material and methods

2.1. SBA-15 and anatoxins

The OMS SBA-15 was synthesized according to Zhao et al. [10]. Briefly, 4 g of Pluronic® P123 ($PEO_{20}PPO_{70}PEO_{20}$, average Mn ~5800), from Sigma-Aldrich, was solubilized in a mixture of deionized water (30 mL) and 120 mL of hydrochloric acid (HCl, ACS reagent, from Synth, 37%) at concentration 2 mol L^{-1}, remaining under magnetic stirring for 1 h at room temperature (25 °C). Then, 8,3 g of tetraethyl orthosilicate, TEOS (from Sigma-Aldrich, 98%), silica source, were added into the mixture at 40 °C and maintained under vigorous magnetic stirring for 24 h. After that step, the solution was placed in an autoclave for hydrothermal treatment at 100 °C for 48 h. Next, the sample was washed with deionized water and dried at 100 °C for 24 h. The triblock copolymer Pluronic® P123 (template) was removed by combining solvent extraction, using ethanol, and calcination under air atmosphere at 540 °C for 6 h. This process is more efficient for template removal than only calcination [25]. The obtained SBA-15 powder was named batch number 11.

The tANA and dANA, produced by the Bioindrustrial Center of Butantan Institute, Brazil, were loaded to SBA-15 at 1:10 protein:silica mass ratio in phosphate-buffered saline (PBS) at pH 7.0. This buffer was used in all measurements of liquid samples.

2.2. Characterization of tANA, SBA-15 and encapsulation studies

Complete SAXS and DLS characterization of dANA in PBS buffer was already reported by our group [24]. The same experimental conditions and data analysis procedure of SAXS, DLS and NAI were used herein. Scanning Electron Microscope (SEM) images were used to check the morphology of the SBA-15 and they were recorded in a JEOL microscope, model JSM 6610LV, operating with a secondary electron imaging (SEI) detector. The SBA-15 sample was placed onto conductive double-sided adhesive carbon tape and covered with a thin layer of gold.

Conventional CD spectra of tANA (0.2 mg/ml) in PBS buffer or encapsulated into SBA-15 were collected in a J-815 CD spectropolarimeter (Jasco, Japan) in a wavelength range from 190 to 280 nm, in 1 nm intervals, using a Suprasil quartz-glass cuvette of 0.1 cm pathlength (Hellma Scientific), at 20 °C, taking an average of six scans per sample. SRCD measurements were collected on the AU-CD beamline at ASTRID2 synchrotron (Aarhus, Denmark) with tANA (20 μM) in PBS buffer over the wavelength range from 170 to 280 nm, in 1 nm intervals, using a 0.0106 cm pathlength quartz cuvette (Hellma Scientific), collecting 3 individual scans per sample, at 20 °C. After all CD/SRCD measurements, final sample spectra were subtracted from the respective buffer baseline, zeroed at 265–270 nm region, and converted to delta epsilon units (using mean residue ellipticity value of 114.7) with CDtoolX software [26]. Final CD spectra deconvolution was estimated with ContinLL algorithms [27], available on Dichroweb server [28], using data set SP175 [29]. FS, used to assess the emission spectrum of the tryptophan residues in tANA (2.0 μM) dispersed in PBS buffer or incorporated into SBA-15, was measured in an ISS K2 fluorimeter (ISS Inc., Champaign, IL) with excitation performed at 295 nm and emission spectra recorded from 305 to 450 nm, in 1 nm intervals, using a 1 cm pathlength quartz cuvette (Hellma Inc, USA). Measurements were taken at 20 °C, controlled by a circulating water bath (Fisher Scientific, USA).

2.3. Animals

Mice phenotypically selected for High (H_{III}) or Low (L_{III}) antibody response, obtained by selective breeding [18], were provided by the Immunogenetics Laboratory of Butantan Institute. Male and female animals at ages ranging from 10 to 12 weeks were used. The experimental protocols were approved by the Ethical Committee of Animal Experimentation at the Butantan Institute (CEUAIB # 2666080319).

2.4. Immunization

H_{III} and L_{III} mice (n = 6 each lineage) were subcutaneously immunized on days 0 and 40 with 10 μg of dANA or tANA encapsulated in 100 μg of SBA-15 (mass ratio 1:10) in a final volume of 200 μL of PBS buffer per dose. Suspensions were kept overnight at 2–8 °C prior to use. Separate groups were also immunized under the same condition but with a mix of the two antigens (dtANA) encapsulated in SBA-15 (10 μg of dANA + 10 μg of tANA in 200 μg of SBA-15). Control groups (n = 3) were immunized with a mixture of 10 μg of each anatoxin dispersed in 200 μL of PBS buffer per dose.

2.5. Antibody titration

Blood samples were collected 10 and 30 days after each immunization dose and serum samples were individually analyzed by ELISA to detect IgG anti-dANA and anti-tANA [24]. Briefly, microplates were coated with dANA (5 μg/mL) or tANA (1 μg/mL) in 0.1 M carbonate/bicarbonate buffer (pH 9.6) and incubated at 37 °C for 2 h. After blocking the reaction with 1% BSA (Sigma-Aldrich) overnight at 4 °C, a washing cycle was performed (Bio-Rad Immunowash, USA), serial dilutions of serum samples were added, and the plate incubated for 1 h at 37 °C. After another washing cycle, peroxidase-labeled anti-mouse IgG (Sigma-Aldrich, 1:7500) was added and plates were then incubated for 1 h at 37 °C. The plates were washed again and the reaction was developed with 0.5 mg/mL o-phenylenediaminedihydrochloride and 0.03% H_2O_2 (Merck) at room temperature. The reaction was stopped with hydrochloric acid 0.2 N and the absorbance was measured at 450 nm. The antibody titers were calculated as the reciprocal serum dilution giving an absorbance of two deviations above the average obtained from a control pool of normal sera and expressed as $[\log_2[x_{mean} \pm SEM]]$.

2.6. Statistical analysis

Bioinformatics analyses were performed using Gor4 [30] software for predictions of secondary structure in tANA. A 3-D homology model was obtained at Swiss-model software [31] using the crystalline structure deposited at PDBID 5N0C as a template, and PDB2CD [32] server was used to obtain a predicted CD spectrum of a 3-D model of tANA. Antibody titer data were expressed as mean ± SEM. Statistical significance of the differences between groups was calculated by one-way ANOVA followed by Tukey's test with the aid of the GraphPad Prism 6. The differences were considered significant for $p \leq 0.05$.

3. Results

3.1. Characterization of tANA, SBA-15 and encapsulation

Fig. 1 shows the SAXS data for tANA particles dispersed in PBS buffer (filled circles). The slope of the curve observed at low q values could be related to interparticle interaction or the presence of large tANA aggregates, as already reported in the literature [33–35]. Because the sample concentration was low (2 mg/mL), the first hypothesis seems unlikely.

Fortunately, it is possible to deal with both effects using the Generalized Indirect Fourier Transform (GIFT) analysis, which evaluates simultaneously the form factor, P(q), related to the size and shape of the protein, and the structure factor, S(q), associated to interpartiLowcle interaction or aggregation [36], the former aspect being our case. Assuming a structure factor of simple globular aggregates with overall radius of gyration Rg_{agg} [37], the satisfactory fitting was performed using the WGIFT program [38], and the result is shown in Fig. 1 (continuous line). From P(q) (dashed line), the pair distance distribution function, p(r), is obtained (inset of Fig. 1), which provides the particle longest length of ~14 nm (where $p(r) \approx 0$) and radius of gyration of $Rg = (4.47 \pm 0.02)$ nm. From the S(q) evaluation, $Rg_{agg} = (19.30 \pm 0.77)$ nm. Using the SAXS curve without the first points (for $q < 0.02$ Å^{-1}) as input to the PRIMUS program [39], the molecular weight of tANA was estimated as ~140 kDa.

The tANA atomic resolution structure has not yet been obtained. Nevertheless, it is possible to compare the experimental SAXS data presented in Fig. 1 to the theoretical scattering of tetanus toxin crystallographic structure (PDBID 5N0C, exhibited in green color in the upper inset of Fig. 2). The comparison was performed using the CRYSOL program [40] and the result is shown in Fig. 2 (green continuous line). The unsatisfactory fitting is expected because the formaldehyde treatment [41], responsible to turn tetanus toxin into tANA anatoxin, promotes changes in the overall protein structure whereas essentially keeps the secondary structure content, as shown by CD analysis presented herein and in agreement with previous works [42]. In addition, pH plays an important role in the tetanus toxin shape: Over a physiological range from 5.0 to 8.0, the higher the pH, the more open the structure [35]. The experimental data for the 5N0C structure was obtained at pH 6.0, then, it is expected to be more packed than it would be at pH 7.0, the same as tANA sample. In this sense, it would be worth it to check if 5N0C pdb model could fit tANA data after suitable "opening" shape modifications. To perform this test, it was used the SREFLEX program [43], which applies normal mode analysis to both estimates the flexibility of protein crystallographic structure and improve its agreement with SAXS data. The satisfactory result is presented in Fig. 2 (red continuous line) and the obtained high-resolution model reasonably agrees with the *ab initio* bead model from DAMMIN program [40] (bottom inset of Fig. 2). SUPALM program [44] was used to superimpose one 3D structure onto another. Therefore, both formaldehyde treatment and pH may introduce important structural changes that explain why the tetanus toxin

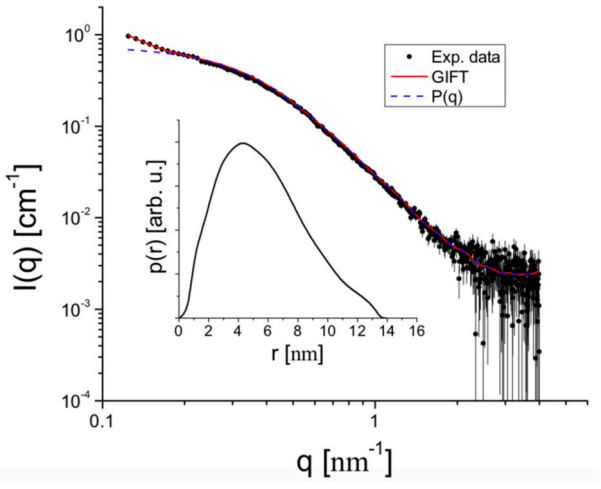

Fig. 1. SAXS data (filled circles) and fitting obtained from WGIFT (red continuous line). The form factor P(q) is also shown (blue dashed line). Inset: p(r) function obtained from P(q). (For interpretation of the references to color in this figure legend, the reader is referred to the Web version of this article.)

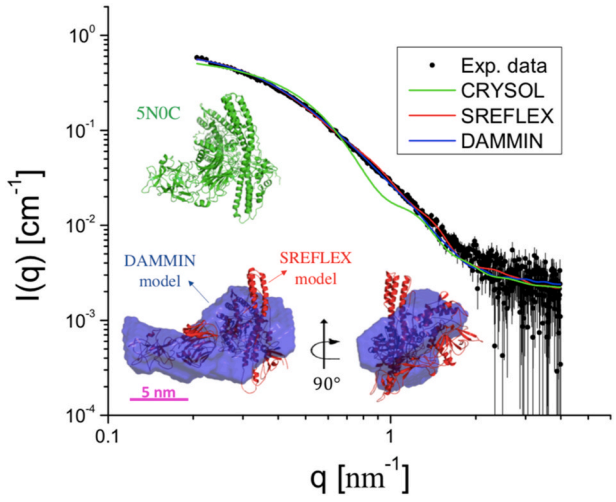

Fig. 2. SAXS data (filled circles) and fittings obtained from CRYSOL (green line), SREFLEX (red line) and DAMMIN (blue line) programs. Inset: Crystallographic structure of tetanus anatoxin, PDB code 5N0C, low-resolution *ab initio* bead model obtained from DAMMIN and high-resolution model obtained from SREFLEX based on 5N0C (PDBID). (For interpretation of the references to color in this figure legend, the reader is referred to the Web version of this article.)

high-resolution model is not suitable to fit tANA SAXS data.

In order to check the presence of tANA aggregates in PBS buffer, DLS was performed and the measured autocorrelation function, C(τ), is shown in Fig. 3 (filled circles). By using the Non-Negatively constrained Least Squares (NNLS) method [45] to satisfactorily fit C(τ) (Fig. 3, continuous line), the histograms of hydrodynamic diameter per intensity, per volume and per number of particles were obtained (Fig. 3, inset). From the histogram of diameter per intensity, it is observed two populations centered at ~10.0 and ~200.0 nm. Despite the existence of the larger particles, they are much less numerous according to the histograms of diameter per volume and per number.

The SAXS results of SBA-15 and SBA-15+anatoxins are depicted in Fig. 4. In all curves is observed well-ordered mesoporous phases with five well-defined diffraction peaks corresponding to the (hkl) Miller indices (100), (110), (200), (210), and (300), attributed to a 2D hexagonal mesoporous structure (*p6mm*), typical of pure SBA-15 [10]. The higher scattered intensity observed for the complexes, mostly at lower q values, is probably associated with the presence of protein aggregates on the silica macropores. Due to this aggregation effect, an increase in the load ratio SBA-15 to anatoxins higher than 1:10 is not recommended.

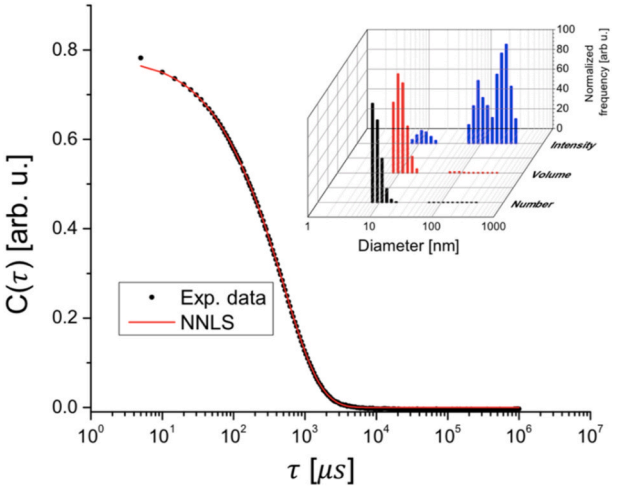

Fig. 3. Autocorrelation function curve (filled circles) fitted by the NNLS method (continuous line). Inset: Hydrodynamic diameter distributions of tANA per number, volume and intensity.

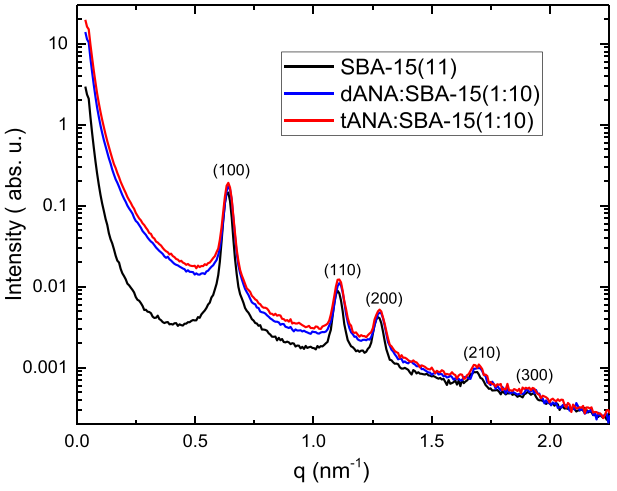

Fig. 4. SAXS of pristine SBA-15 and the same silica encapsulated with dANA and tANA.

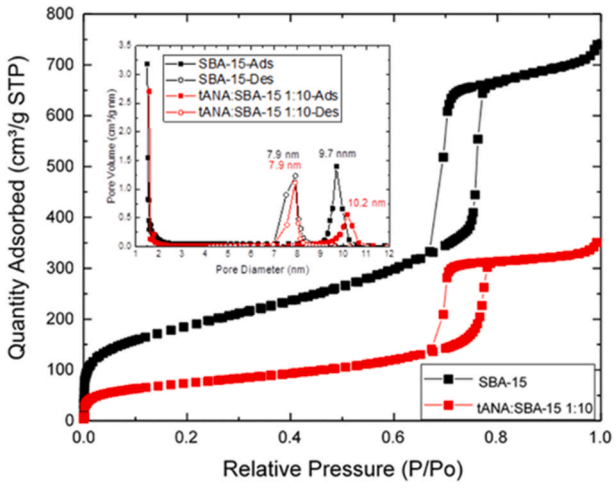

Fig. 5. NAI of pure SBA-15 and with tANA encapsulated at 1:10 mass ratio. Inset: Pore size distribution of the same two samples taken from adsorption and desorption branches.

Fig. 5 shows the NAI results obtained for pristine SBA-15 and SBA-15 containing tANA encapsulated at 1:10 mass ratio. After encapsulation, the surface area and pore volume decreased from 668 $m^2\ g^{-1}$ to 267 $m^2\ g^{-1}$ and from 1.39 $cm^3\ g^{-1}$ to 0.70 $cm^3\ g^{-1}$, respectively, suggesting that tANA is retained in the silica matrix.

Fig. 6 shows the SEM imagens of pristine SBA-15 particles. SBA-15 particles have a typical interconnected rod-like morphology, with uniform size, forming aggregates in a wheat-like macrostructure, as reported by Zhao et al. [10].

Secondary structure predictions of tANA based on its primary structure suggest that the protein is arranged in 29% α-helix, 19% β-strands, and 52% disordered, as shown in Supplementary Fig. 1. In agreement with such analysis, the 3D structure deposited at PDBID 5N0C for the tetanus toxin total length protein shows the content of secondary structure arranged as 28.4% in α-helix, 22.1% in β-strands, and 49.6% others (disordered, turns).

The predicted CD spectrum of tANA (entry 5N0C), shown in Fig. 7, is typical of a protein with mixed alpha/beta/disordered content due to the low spectral magnitude of the peaks and the two asymmetric minima presented at 220 and 208 nm. Moreover, the theoretical spectrum is in agreement with the corresponding experimental spectra.

The SRCD spectrum of tANA in PBS (pH 7.0) presents quite equivalent spectral lineshape to that seen on the CD spectrum of this anatoxin incorporated in SBA-15 particles (1:10), with two negative bands at 222 and 208 nm of different intensities (with the 208 nm band being more pronounced), and a positive peak at the 192 nm region (Fig. 7). Besides, it is possible to observe a negative band at 175 nm in the SRCD spectrum of tANA in PBS, which is assigned to the β-strand content of the protein [46]. The similar spectra suggest the preservation of protein secondary structure in the process of incorporation into the mesoporous particle. Estimates of secondary structure with the SRCD spectrum of tANA gave 28% α-helix, 19% β-strands, and 53% in other structures.

An additional negative band at 170 nm is clearly seen on the SRCD spectrum of the dehydrated film of tANA. The SRCD spectrum of the anatoxin on a partially dehydrated film is equivalent to the one obtained in solution. Such similarity is in agreement with the preservation of tANA secondary structure in the process of film formation (by dehydration).

The fluorescence spectrum of Tryptophan (Trp) residues in tANA (0.1 mg/ml in PBS) was quite similar to that of the protein incorporated into SBA-15 (Fig. 8), presenting maximum emission centered at ~326

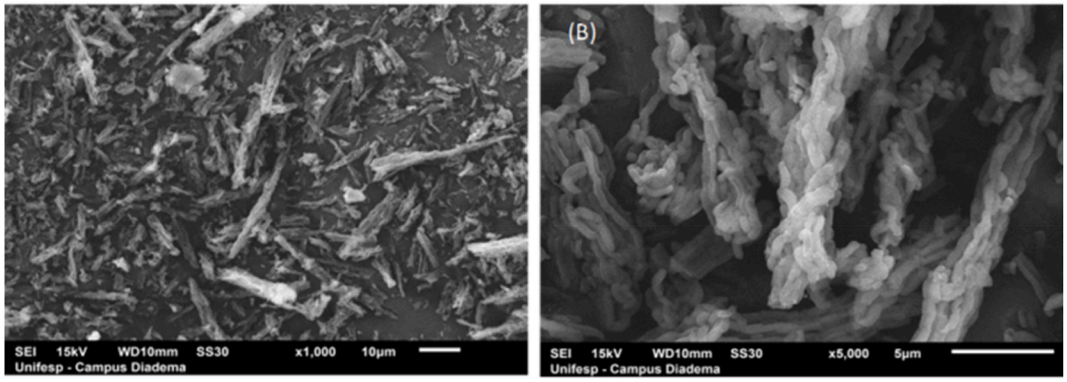

Fig. 6. SEM images of pure SBA-15 at different magnifications: (A) = x 1000 and (B) = x 5000.

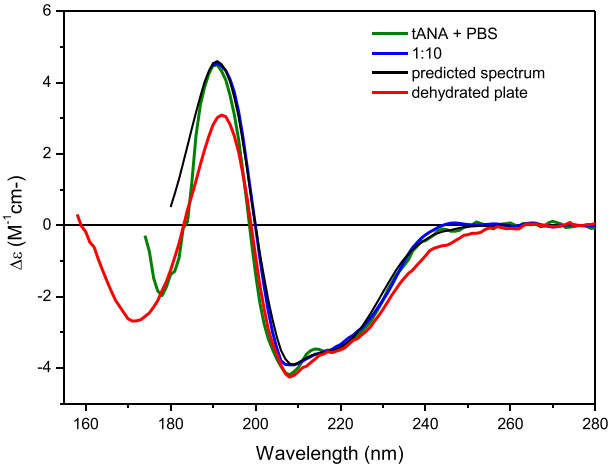

Fig. 7. SRCD spectrum of tANA in PBS (green) and its CD spectrum when incorporated into SBA-15 (blue) at 1:10 mass ratio. Theoretical CD spectrum of tANA (black) and SRCD spectrum of a partially dehydrated film of the anatoxin deposited on a quartz plate (red).

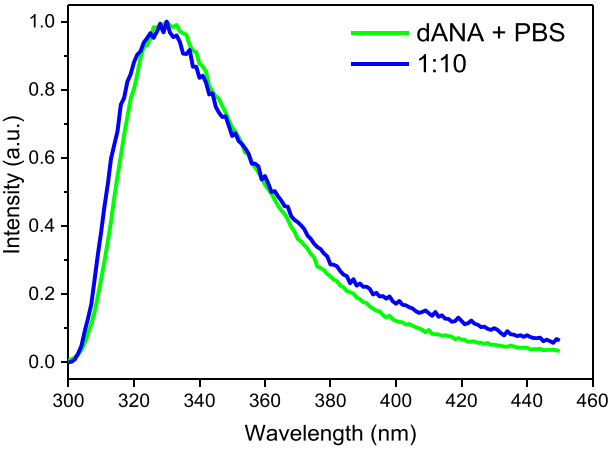

Fig. 8. Normalized fluorescence spectrum of Trp residues of tANA in PBS (green) and incorporated into SBA-15 particles (blue) at 1:10 mass ratio. (For interpretation of the references to color in this figure legend, the reader is referred to the Web version of this article.)

nm, indicating the preservation of both the aromatic residues from exposure with the polar solvent and the aromatic microenvironment after the protein incorporation into the silica.

3.2. Effect of SBA-15 on modulation of antibody response after immunization with combination dANA and tANA vaccine

To evaluate the role of SBA-15 as an adjuvant, both H_{III} e L_{III} mice were immunized with two doses of dtANA antigens encapsulated or not in SBA-15. Individual anti-dANA and anti-tANA specific IgG were titrated in the serum from blood samples collected 10 and 30 days after each immunization dose. Anti-dANA IgG titers of H_{III} mice (blue lines) that received or not SBA-15 (Fig. 9A) were similar 10 days after the booster (SR 10) and so remained until the thirtieth day (SR 30). For the L_{III} mice, the use of SBA-15 significantly increased anti-dANA IgG titers (Fig. 9A) reaching levels similar to those of H_{III} animals throughout the study period. This phenomenon was also observed in the anti-tANA IgG response (Fig. 9B) for H_{III} and L_{III} mice during the secondary response (SR 10 and SR 30).

3.3. Antibody response after dANA and tANA administered individually or in combination

To determine if the mixture of the two anatoxins is more effective to induce specific IgG antibodies against dANA and tANA than individual immunization, groups of H_{III} and L_{III} mice were immunized with dANA or tANA individually encapsulated in SBA-15 and compared to groups immunized with the both antigens in combination encapsulated in SBA-15. Blood samples were collected 10 and 30 days after each immunization dose, and serum samples were tested by ELISA. A similar anti-dANA IgG production occurred after immunization with individual dANA or combined dtANA in both mouse lines (Fig. 10A). However, dtANA was more potent to stimulate anti-tANA IgG antibodies than individual tANA in both H_{III} and L_{III} mice groups (Fig. 10B).

4. Discussion

We analyzed the effectiveness of subcutaneous immunization with diphtheria (dANA), tetanus (tANA) anatoxins, and dtANA combination, encapsulated in SBA-15 in mice selected for their high (H_{III}) or low (L_{III}) antibody response. SBA-15 has been widely used in vaccine efficacy studies due to the physical and structural properties that allow it to encapsulate several antigens without damaging their protein structure, promoting a more effective immune response in either subcutaneous or oral immunization [13–15,24]. There are few adjuvants approved for

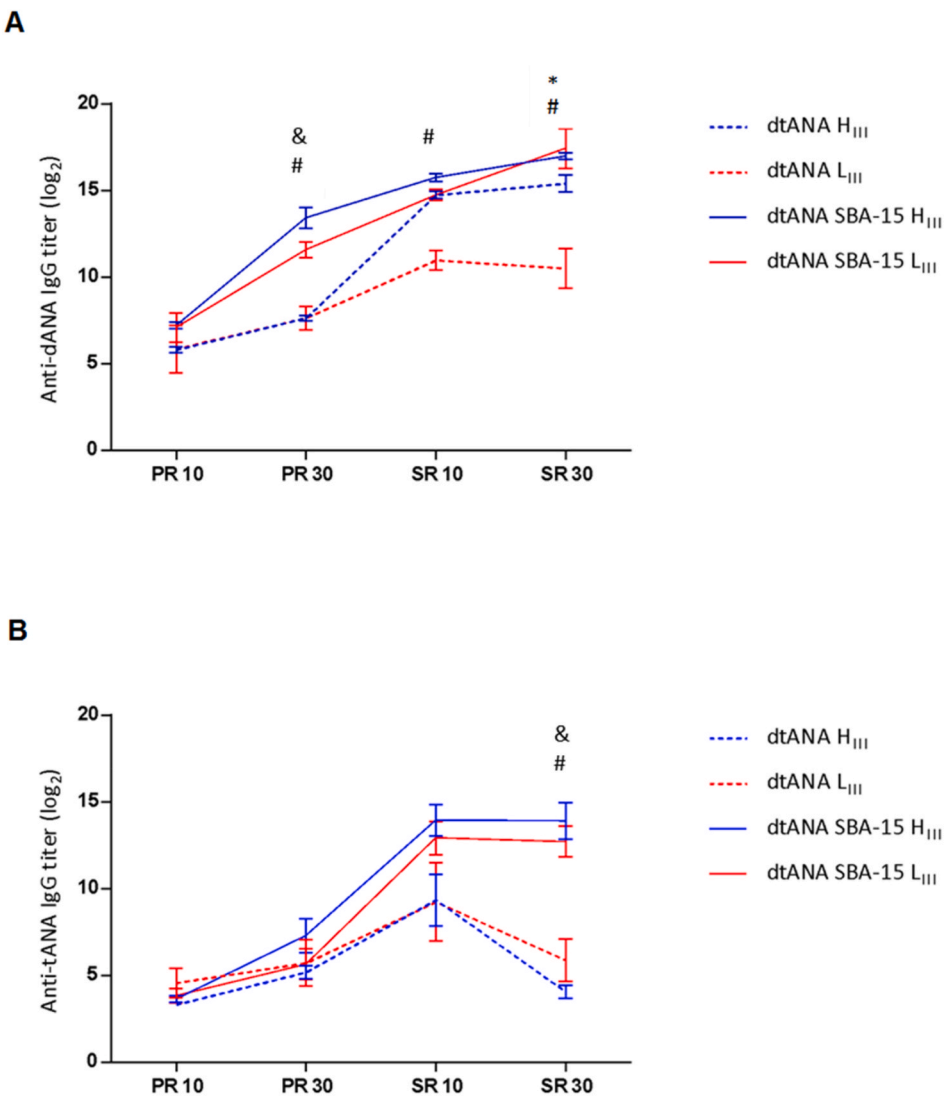

Fig. 9. IgG antibody production by H_{III} e L_{III} mice after combined dANA and tANA immunization with or without SBA-15. **(A)** Anti-dANA antibodies, **(B)** anti-tANA antibodies. **PR 10** – primary antibody response, 10 days after first dose; **PR 30** – primary antibody response, 30 days after first dose; **SR 10** – secondary antibody response, 10 days after second dose; **SR 30** – secondary antibody response, 30 days after second dose. Blue lines: H_{III} mice; Red lines: L_{III} mice; discontinuous lines: only antigens; continuous lines:antigens plus SBA-15 ($p \leq 0.05$, # dtANA L_{III} vs dtANA SBA-15 L_{III}; **&** dtANA H_{III} vs dtANA SBA-15 H_{III}; *dtANA L_{III} vs dtANA H_{III}). (For interpretation of the references to color in this figure legend, the reader is referred to the Web version of this article.)

human use like calcium phosphate and aluminum salts [4, 5, 47]. Aluminum salts present some significant side effects as swelling, induration, erythema, induction of allergy and autoimmune reaction [4,5,8, 48]. SBA-15 silica is a promising adjuvant candidate given its intrinsic and useful properties. Its low toxicity was demonstrated by propidium iodide staining assays using macrophages [14], Besides, no traces of silica were found in the liver and spleen of animals injected with silica by oral or intramuscular route and no toxicity was observed. It was also demonstrated that silica degradation occurred naturally in the body over a period of time [49,50].

Regarding the physical characterization of tANA, it was possible to determine, from SAXS analysis, the pair distribution function p(r) profile (Fig. 1, inset), which suggests a globular and slightly elongated shape for the protein, with longest length of ~14 nm, radius of gyration of R_g = (4.47 ± 0.02) nm and molecular weight of ~140 kDa, all results in agreement with previous studies [42]. The most extended length of tANA is larger than the silica mesopores (~10 nm), therefore its incorporation is expected to be in the macropores of the silica matrix. In addition, mesopore blockage can occur, which can be reflected on the decrease of the surface area and pore volume detected by the NAI results (Fig. 5). Moreover, the aggregates responsible for the slope of the SAXS curve at low q values (Fig. 1) have R_{agg} = (19.30 ± 0.77) nm, leading to the conclusion that tANA monomers coexist with large oligomers. In all subsequent analyses using CRYSOL, SREFLEX and DAMMIN programs (Fig. 2), the first points of the SAXS curve corresponding to those oligomers ($q < 0.2\ nm^{-1}$) were not considered because they interfere in the modeling outcomes.

It is interesting to note that even if the longest length of tANA is ~14 nm, evidenced by the p(r) function, a quick inspection in the obtained bead model (Fig. 2) leads to the conclusion that other dimensions have a length of ~10 nm or less, thus permitting the protein encapsulation inside the SBA-15 mesopores. However, this loading process is expected to be more difficult than for other smaller antigens, such as diphtheria anatoxin [24]. Additionally, the size distribution of hydrodynamic diameter per intensity, obtained from DLS measurements (Fig. 3), corroborate the conclusion, from SAXS analyses, that tANA coexists with its oligomeric forms.

The SAXS and NAI results of SBA-15+tANA suggest that a fraction of the antigens are encapsulated inside the SBA-15 mesopores, while the remaining part is probably protected inside SBA-15 macropores. This effect is likely more pronounced for tANA, which is larger than dANA, whose physicochemicals characteristics have already been published by our group [24].

Another important finding was related to the integrity of tANA structure after encapsulation either inside the meso- or macropores, confirmed by CD, SRCD and FS, being a guarantee that it can still induce the formation of antibodies.

Due to the size of the tANA [33,34] it mainly stands in the silica

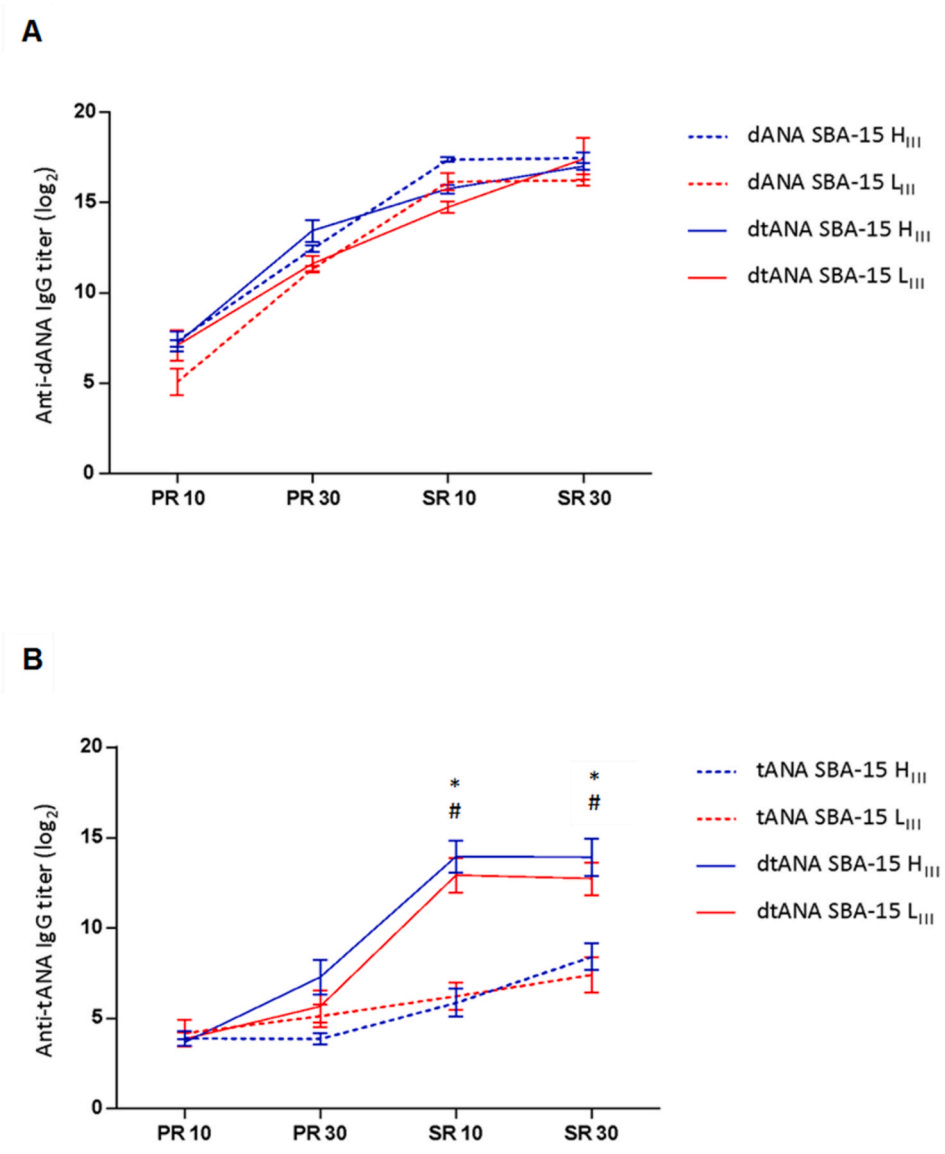

Fig. 10. IgG antibody production by H_{III} e L_{III} mice after combined or individual dANA and tANA immunization with SBA-15. **(A)** Anti-dANA antibodies, **(B)** anti-tANA antibodies. **PR 10** – primary antibody response, 10 days after first dose; **PR 30** – primary antibody response, 30 days after first dose; **SR 10** – secondary antibody response, 10 days after second dose; **SR 30** – secondary antibody response, 30 days after second dose. Blue lines: H_{III} mice; Red lines: L_{III} mice; discontinuous lines: only antigens; continuous lines:antigens plus SBA-15 ($p \leq 0.05$, # tANA SBA-15 L_{III} vs dtANA SBA-15 L_{III}; *tANA SBA-15 H_{III} vs dtANA SBA-15 H_{III}). (For interpretation of the references to color in this figure legend, the reader is referred to the Web version of this article.)

macropores, as evidenced by SAXS and NAI analysis. We believe that higher levels of anti-tANA could be achieved if silica particles with larger pores were used. On the other hand, L_{III} mice are low antibody responders to multiple antigens, phenomena known as multispecific effects [51]. Despite their low humoral response, under the SBA-15 adjuvanticity these mice responded with equivalent titers to H_{III} ones for both antigens, corroborating data previously obtained by our group [13,14].

It has been shown that the vaccination with mixture of tetanus and diphtheria antigens using aluminum as an adjuvant enhances the production of antibodies against tetanus when compared with tetanus vaccine alone [52,53]. In the present work, we intended to explore if this would also happen in the presence of another type of adjuvant, the nanostructured silica SBA-15. We found a significant increase in response to tANA in H_{III} and L_{III} mice when immunized with dtANA encapsulated in SBA-15, indicating an adjuvant effect of diphtheria in the antigen association protocol using SBA-15.

Capacity of incorporating proteins characteristics and several kinds of proteins have been loaded to SBA-15 including BSA [8,54], Lysozyme [55], Myoglobine [56], intimin and snake venon [13] for a variety of applicaton. A possible mechanism by which SBA-15 can enhance the immune response could be the depot effect [54,57], which increases the antigen permanence at the injection site since the proteins inside the silica are released slowly, prolonging the period of interaction of the antigen with the immune system. Furthermore, the SBA-15 improve their uptake by the professional antigen presenting cells (APC) where the antigens are delivered [58]. Together with these characteristics, SBA-15 also can give a mixed response pattern with both TH1 and TH2 type responses, often desirable in vaccination [58].

This study demonstrates that ordered mesoporous silica SBA-15 retains tANA antigens in its matrix, preserving their properties and stimulating antibody production after a subcutaneous vaccination schedule. It has also shown that immunization with such formulation provides a better anti-tANA antibodies response for both H_{III} and L_{III} mice. More importantly, our study demonstrates that immunization with dtANA encapsulated in SBA-15 induced antibody titers in L_{III} mice similar to those observed in H_{III} mice, demonstrating the efficacy of SBA-15 as adjuvant in our model (Fig. 9). It is also important to highlight that unlike other authors that have used only the C chain of the molecule of tetanus anatoxin encapsulated in silica [59,60], we have used all the 3 chains, A, B and C in our vaccine. Therefore, we show for the first time the encapsulation of the whole tANA molecule in SBA-15 and the effect of this immunogenic complex on subcutaneous immunizations.

In conclusion, our data supports the use of SBA-15 as a suitable

adjuvant in the production of vaccines. Furthermore, since the antigen is encapsulated, SBA-15 can potentially provide protection to the proteins from the external environment during the passage through the gastro-intestinal tract, being an antigen vehicle for oral vaccination schemes.

Funding

This work was supported by São Paulo Research Foundation - FAPESP (Projects number 2017/17844-8; 2019/12301-1; 2020/13204-7).

Declaration of competing interest

The authors declare that they have no known competing financial interests or personal relationships that could have appeared to influence the work reported in this paper.

Acknowledgments

CNPq is acknowledged by the fellows C.L.P.O, J.L.S.L, M.C.A.F. and O.A.S.

Appendix A. Supplementary data

Supplementary data to this article can be found online at https://doi.org/10.1016/j.biologicals.2022.10.001.

References

[1] Tiwari TSP, Wharton M Diphtheria Toxoid. Plotkin SA. In: Orenstein WA, Offit PA, Edwards KM, editors. Plotkin's vaccine. Philadelphia: Elsevier; 2018. 261–75e7. https://doi.org/10.1016/b978-0-323-35761-6.00019-5.
[2] Yen LM, Thwaites CL. 20 Tetanus. Lancet 2019;393:10181. https://doi.org/10.1016/S0140-6736(18)33131-3. Epub 2019 Mar 29. Erratum in: Lancet. 2019 Apr 27;393(10182):1698. PMID: 30935736.
[3] Shi S, Zhu H, Xia X, Liang Z, Ma X, Sun B. Vaccine adjuvants: understanding the structure and mechanism of adjuvanticity. Vaccine 2019;37:3167–78. https://doi.org/10.1016/j.vaccine.2019.04.055.
[4] Aggerbeck H, Heron I. Adjuvanticity of aluminium hydroxide and calcium phosphate in diphtheria-tetanus vaccines-I. Vaccine 1995;13(14):1360–5. https://doi.org/10.1016/0264-410x(94)00081-w.
[5] Aggerbeck H, Fenger C, Heron I. Booster vaccination against diphtheria and tetanus in man. Comparison of calcium phosphate and aluminium hydroxide as adjuvants-II. Vaccine 1995;13(14):1366–74. https://doi.org/10.1016/0264-410x(94)00082-x.
[6] Lindblad EB. Aluminium adjuvants-in retrospect and prospect. 27-28 Vaccine 2004;2004(22). https://doi.org/10.1016/j.vaccine.2004.03.032. 3658–68.
[7] Danielsson R, Eriksson H. Aluminium Adjuvants in Vaccines - a way to modulate the immune response. Semin Cell Dev Biol 2021;115:3–9. https://doi.org/10.1016/j.semcdb.2020.12.008.
[8] He P, Zou Y, Hu Z. Advances in aluminum hydroxide-based adjuvant research and its mechanism. Hum Vaccines Immunother 2015;11(2):477–88. https://doi.org/10.1080/21645515.2014.1004026.
[9] Grun JL, Maurer PH. Different T helper cell subsets elicited in mice utilizing two different adjuvant vehicles: the role of endogenous interleukin 1 in proliferative responses. Cell Immunol 1989;121(1):134–45. https://doi.org/10.1016/0008-8749(89)90011-7. PMID: 2524278.
[10] Zhao DY, Feng JL, Huo QS, Melosh N, Fredrickson GH, Chmelka BF, et al. Triblock copolymer syntheses of mesoporous silica with periodic 50 to 300 angstrom pores. Science 1998;29(5350):548–52. https://doi.org/10.1126/science.279.5350.548.
[11] Mody KT, Popat A, Mahony D, Cavallaro AS, Yu CZ, Mitter N. Mesoporous silica nanoparticles as antigen carriers and adjuvantsfor vaccine delivery. Nanoscale 2013;5(12):5167–79. https://doi.org/10.1039/c3nr00357d.
[12] Mahony D, Cavallaro AS, Stahr F, Mahony TJ, Qiao SZ, Mitter N. Mesoporous silica nanoparticles act as a self-adjuvant for ovalbumin model antigen in mice. Small 2013;9(18):3138–46.
[13] Mercuri LP, Carvalho LV, Lima FA, Quayle C, Fantini MCA, Tanaka GS, et al. Ordered mesoporous silica SBA-15: a new effective adjuvant to induce antibody response. Small 2006;2(2). https://doi.org/10.1002/smll.200500274. 254–56.
[14] Carvalho LV, Ruiz RC, Scaramuzzi K, Marengo EB, Matos JR, Tambourgi DV, et al. Immunological parameters related to the adjuvant effect of the ordered mesoporous silica SBA-15. Vaccine 2010;29. https://doi.org/10.1016/j.vaccine.2010.09.087. 7829-36.
[15] Scaramuzzi K, Oliveira DCA, Carvalho LV, Tambourgi DV, Tenório ECN, Rizzi M, et al. Nanostructured SBA-15 Silica as an adjuvant in immunizations with Hepatitis B vaccine. Einstein 2011;9(4). https://doi.org/10.1590/s1679-45082011ao2162. 436–41.
[16] Biozzi G, Mouton D, Sant'Anna AO, Passos HC, Gennari M, Reis MH, et al. Genetics of immunoresponsiveness to natural antigens in the mouse. Curr Top Microbiol Immunol 1979;85:31–98.
[17] Sant'Anna OA, Ferreira VC, Reis MH, Gennari M, Ibañez OM, Esteves MB, et al. Genetic parameters of the polygenic regulation of antibody responsiveness to flagellar and somatic antigens of salmonellae. J Immunogenet 1982;9(3):191–205. https://doi.org/10.1111/j.1744-313x.1982.tb00791.x.
[18] Siqueira M, Bandieri A, Reis MS, Sant'anna OA, Biozzi G. Selective breeding of mice for antibody responsiveness to flagellar and somatic antigens of salmonellae. Eur J Immunol 1976;6(4). https://doi.org/10.1002/eji.1830060403. 241–9.
[19] Mouton D, Claude S, Biozzi G. Genetic regulation of high and low immunoresponsiveness. In: Gershwin ME, Merchant B, editors. Immunologic defects in laboratory animals. New York: Plenum Press; 1981. p. 19–47. 00110.1007/978-1-4757-0325-2.
[20] Mancuso RI, Miyaji EN, Silva CCF, Portaro FV, Soares-Schanoski A, Ribeiro OG, et al. Impaired expression of CXCL5 and matrix metalloproteinases in the lungs of mice with high susceptibility to Streptococcusp neumoniae infection. Immunity, Inflammation and Disease 2018;6(1). https://doi.org/10.1002/iid3.205. 128–42.
[21] Vorraro F, Cabrera WHK, Ribeiro OG, Jensen JR, De Franco M, Ibañez OM, et al. Trypanosoma Cruzi infection in genetically selected mouse lines: genetic linkage with Quantitative Trait Locus controlling antibody response. Mediat Inflamm 2014:952857. https://doi.org/10.1155/2014/952857.
[22] Sant'Anna OA, Massa S, Mouton D, Bouthillier Y, Mevel JC, Ibañez OM, et al. Salmonella Typhimurium infection in High and Low antibody responder mice: inverse correlation between antibody responsiveness and resistance to infection. FEMS (Fed Eur Microbiol Soc) Microbiol Lett 1989;1(8–9). https://doi.org/10.1111/j.1574-6968.1989.tb02437.x. 465-72.
[23] Mouton D, Parant M, Mevel JC, Parant F. Dose-dependent efficacy of vaccination against K. Pneumoniae in High and Low antibody responder lines of mice. Immunol Lett 1987;14(4). https://doi.org/10.1016/0165-2478(87)90015-0. 335–9.
[24] Rasmussen MK, Bordallo HN, Bordenalli MA, Akamatsu MA, Trezena AG, Tino-De-Franco M, et al. Assessing the efficiency of SBA-15 as a nanocarrier for diphtheria anatoxin. Microporous Mesoporous Mater 2021;312:1–9. https://doi.org/10.1016/j.micromeso.2020.110763.
[25] Losito DW, Lopes PS, Ueoka AR, Fantini MCA, Oseliero-Filho PL, Andréo-Filho N, et al. Biocomposites based on SBA-15 and papain: characterization, enzymatic activity and cytotoxicity evaluation. Microporous Mesoporous Mater 2021;325:111316. https://doi.org/10.1016/j.micromeso.2021.111316.
[26] Miles AJ, Wallace BA. CDtoolX, a downloadable software package for processing and analyses of circular dichroism spectroscopic data. Protein Sci 2018;27(9):1717–22. https://doi.org/10.1002/pro.3474.
[27] van Stokkum IH, Spoelder HJ, Bloemendal M, van Grondelle R, Groen FC. Estimation of protein secondary structure and error analysis from circular dichroism spectra. Anal Biochem 1990;191(1):110–8. https://doi.org/10.1016/0003-2697(90)90396-q.
[28] Whitmore L, Wallace BA. DICHROWEB, an online server for protein secondary structure analyses from circular dichroism spectroscopic data. Nucleic Acids Res 2004;32:W668–73. https://doi.org/10.1093/nar/gkh371.
[29] Lees JG, Miles AJ, Wien F, Wallace BA. A reference database for circular dichroism spectroscopy covering fold and secondary structure space. Bioinformatics 2006;22(16):1955–62. https://doi.org/10.1093/bioinformatics/btl327.
[30] Garnier J, Gibrat JF, Robson B. GOR method for predicting protein secondary structure from amino acid sequence. Methods Enzymol 1996;266:540–53. https://doi.org/10.1016/S0076-6879(96)66034-0.
[31] Waterhouse A, Bertoni M, Bienert S, Studer G, Tauriello G, Gumienny R, et al. SWISS-MODEL: homology modelling of protein structures and complexes. Nucleic Acids Res 2018;46(W1):W296–303. https://doi.org/10.1093/nar/gkh371 [ ] Whitmore L, Wallace BA. DICHROWEB: an online server for protein secondary structure analyses from circular dichroism spectroscopic data. Nucleic acids research 2004;32:W668–W673.
[32] Mavridis L, Janes RW. PDB2CD: a web-based application for the generation of circular dichroism spectra from protein atomic coordinates. Bioinformatics 2017;33:56–63. https://doi.org/10.1093/bioinformatics/btw554.
[33] Costantino HRS, Schwendeman P, Griebenow K, Klibanov AM, Langer R. The secondary structure and aggregation of lyophilized tetanus toxoid. J Pharmaceut Sci 1996;85(12):1290–3. https://doi.org/10.1021/js960148+.
[34] Jain NK, Roy I. Accelerated stability studies for moisture-induced aggregation of tetanus toxoid. Pharmaceutical Research 2011;28(3):626-39 2011. https://doi.org/10.1007/s11095-010-0316-2.
[35] Masuyer G, Conrad J, Stenmark P. The structure of the tetanus toxin reveals pH-mediated domain dynamics. EMBO Rep 2017;18(8):1306–17. https://doi.org/10.15252/embr.201744198.
[36] Bergmann A, Fritz G, Glatter O. Solving the generalized indirect Fourier transformation (GIFT) by Boltzmann simplex simulated annealing (BSSA). J Appl Crystallogr 2000;33:1212–6. https://doi.org/10.1107/S0021889800008372.
[37] Oliveira CLP, Monteiro AM, Figueiredo Neto AM. Structural modifications and clustering of low-density lipoproteins in solution induced by heating Brazilian. J Phys 2014;44:753–64.
[38] Oliveira CLP, Behrens MA, Pedersen JS, Erlacher K, Otzen D, Pedersen Js J. A SAXS study of glucagon fibrillation. J Mol Biol 2009;387(1):147–61. https://doi.org/10.1016/j.jmb.2009.01.020.
[39] Konarev PV, Volkov VV, Sokolova AV, Koch MHJ, Svergun DI. Primus - a Windows-PC based system for small-angle scattering data analysis. J Appl Crystallogr 2003;36:1277–82. https://doi.org/10.1016/j.jmb.2009.01.020.

[40] Svergun DI. Restoring low resolution structure of biological macromolecules from solution scattering using simulated annealing. Biophys J 1999;76(6):2879–86. https://doi.org/10.1016/S0006-3495(99)77443-6. Erratum in: Biophys J. 1999; 77(5):2896. PMID: 10354416; PMCID: PMC1300260.
[41] Puchtler H, Meloan SN. On the chemistry of formaldehyde fixation and its effects on immunohistochemical reactions. Histochemistry 1985;82:201–4. https://doi.org/10.1007/BF00501395.
[42] Alsarraf H, Dedic E, Bjerrum MJ, Ostergaard O, Kristensen MP, Petersen JW, et al. Biophysical comparison of diphtheria and tetanus toxins with the formaldehyde-detoxified toxoids, the main components of diphtheria and tetanus vaccines. Virulence 2017;8:1880–9. https://doi.org/10.1080/21505594.2017.1321726.
[43] Panjkovich A, Svergun DI. Deciphering conformational transitions of proteins by small angle X-ray scattering and normal mode analysis. Phys Chem Chem *Phys* 2016;18:5707–19. https://doi.org/10.1039/C5CP04540A.
[44] Konarev PV, Petoukhov MV, Svergun DI. Rapid automated superposition of shapes and macromolecular models using spherical harmonics. J Appl Crystallogr 2016; 49:953–60. https://doi.org/10.1107/S1600576716005793.
[45] Morrison ID, Grabowski EF, Herb CA. Improved techniques for particle-size determination by quasi-elastic light-scattering. Langmuir 1985;1:496–501. https://doi.org/10.1021/la00064a016.
[46] Wallace BA. Protein characterization by synchrotron radiation circular dichroism spectroscopy. Q Rev Biophys 2009;42(4):317–70. https://doi.org/10.1017/S003358351000003X.
[47] Braun LJ, Clapp T, Siebert P, Chen DX. Vaccines with aluminum-containing adjuvants: optimizing vaccine efficacy and thermal stability. J Pharmacol Sci 2011; 100(2):388–401. https://doi.org/10.1002/jps.22284.
[48] van der Laan JW, Gould S, Tanir JY. Safety of vaccine adjuvants: focus on autoimmunity. Vaccine 2015;33(15). https://doi.org/10.1016/j.vaccine.2015.01.073. 1507-14.
[49] Huang X, Young NP, Townley HE. Characterization and comparison of mesoporous silica particles for optimized drug delivery. Nanomater Nanotechnol 2014;4:1–15. https://doi.org/10.5772/58290.
[50] Mariano-Neto F, Matos JR, Cides da Silva LC, Carvalho LV, Scaramuzzi K, Sant'Anna OA, Oliveira CP, Fantini MCA. Physical properties of ordered mesoporous SBA-15 silica as immunological adjuvant. J Phys D Appl Phys 2014;47: 1–10.
[51] Ibanez OM, Mouton D, Silvio LO, Ribeiro OG, Piatti RM, Sant'Anna OA, et al. Polygenic Control of quantitative antibody responsiveness: restrictions of the multispecific effect related to the selection antigen. Immunogenetics 1988;28(1): 6–12. https://doi.org/10.1007/bf00372523.
[52] Miller JJ, Saito TM. Concurrent immunization against tetanus, diphtheria, and pertussis: a comparison of fluid and alum-precipitated toxoids. J Pediatr 1942;21 (1):31–44. https://doi.org/10.1016/S0022-3476(42)80202-4.
[53] Greenberg L, Flemings DS. Increased efficiency of diphtheria toxoid when combined with pertussis vaccine: a preliminary. Can J Public Health/Revue Canadienne de Sante'e Publique. 1947;38(6):279–82.
[54] Wang T, Jiang H, Zhao Q, Wang S, Zou M, Cheng G. Enhanced mucosal and systemic immune responses obtained by porous silica nanoparticles used as an oral vaccine adjuvant: effect of silica architecture on immunological properties. Int J Pharm 2012;15(1–2):351–8. https://doi.org/10.1016/j. 436.
[55] Lee JW, Tra PT, Kim SI, Roh SH. Adsorption properties of proteins on SBA-15 nanoparticles functionalized with aminosilanes. J Nanosci Nanotechnol 2008;8 (10):5152–7. https://doi.org/10.1166/jnn.2008.1206.
[56] Cheng K, El-Boubbou K, Landry CC. Binding of HIV-1 gp120 glycoprotein to silica nanoparticles modified with CD4 glycoprotein and CD4 peptide fragments. ACS Appl Mater Interfaces 2012;4(1):235–43. https://doi.org/10.1021/am2013008.
[57] Kupferschmidt N, Qazi KR, Kemi C, Vallhov H, Garcia-Bennett AE, Gabrielsson S, et al. Mesoporous silica particles potentiate antigen-specific T-cell responses. Nanomedicine 2014;9(12):1835–46. https://doi.org/10.1107/S1600576716005793.
[58] Vallhov H, Kupferschmidt N, Gabrielsson S, Paulie S, Strømme M, Garcia-Bennett AE, Scheynius A. Adjuvant properties of mesoporous silica particles tune the development of effector T cells. Small 2012;8(13):2116–24. https://doi.org/10.1002/smll.201102620.
[59] Doekhie A, Dattani R, Chen YC, Yang Y, Smith A, Silve AP, Koumanov F, Wells SA, Edler KJ, Marchbank KJ, van den Elsen JMH, Sartbaeva A. Ensilicated tetanus antigen retains immunogenicity: in vivo study and time-resolved SAXS characterization. Sci Rep 2020;10:9243. https://doi.org/10.1038/s41598-020-65876-3.
[60] Chen YC, Smith T, Hicks RH, Doekhie A, Koumanov F, Wells SA, Edler KJ, van den Elsen J, Holman GD, Marchbank KJ, Sartbaeva A. Thermal stability, storage and release of proteins with tailored fit in silica. Sci Rep 2017;24(7):46568. https://doi.org/10.1038/srep46568.